Journal of Molecular Liquids 347 (2022) 118316

Contents lists available at ScienceDirect

Journal of Molecular Liquids

journal homepage: www.elsevier.com/locate/molliq

Novel sampling procedure and statistical analysis for the thermal characterization of ionic nanofluids

A. Svobodova-Sedlackova [a,b], C. Barreneche [a], P. Gamallo [a,b], A. I. Fernández [a,*]

[a] Departament de Ciència de Materials i Química Física, Universitat de Barcelona, C/Martí i Franqués 1, 08028, Barcelona, Spain
[b] Institut de Química Teòrica i Computacional, IQTC-UB, Universitat de Barcelona, C/Martí i Franqués 1, 08028, Barcelona, Spain

ARTICLE INFO

Article history:
Received 13 September 2021
Revised 26 November 2021
Accepted 8 December 2021
Available online 13 December 2021

Keywords:
Nanofluids
Thermal Energy System (TES)
Nanoparticles
Specific Heat Capacity (C_p)
Sampling

ABSTRACT

An efficient storage system is crucial for the effective implementation of renewable energies in the energy ecosystem, required to mitigate the climate change and to reach the European Green Deal. Nanofluids features improved thermal properties, being able to store unexpected amount of energy by adding around 1 wt% nanoparticles at the base fluid. Therefore, nanofluids become more attractive for their implementation as Thermal Energy Storage (TES) medium or Heat Transfer Fluid (HTF). However, the main drawbacks of nanofluids are the lack of consensus on a theoretical explanation of this behaviour, and the controversial lack of uniformity of the thermophysical experimental results in the literature. The goal of this work is to develop and perform a study of the thermophysical properties of several nanofluid samples and the subsequent statistical analysis. To achieve this objective, three batches of 24-samples were analysed: $NaNO_3$ based nanofluids with three types of nanoparticles (1% wt.): SiO_2, Al_2O_3 and clay. The statistical analysis indicates that nanoparticles have a low impact in the melting enthalpy and melting temperature and a strong impact in the specific heat capacity (C_p). The most remarkable result is the high dispersion of C_p values despite considering the sampling procedure. This fact agrees with the high variability of results found in the literature. Finally, the methodology proposed in this work may facilitate the comparison among measured results and literature results.

1. Introduction

Nanofluids (NFs) are a colloidal suspension of nanoparticles (NPs) in a liquid medium that were originally introduced by Choi S.U. et al. in 1995 [1]. Since then and up to 2021, almost eighteen thousand articles related to this field have been published. One of the most studied topic is the enhancement of thermophysical properties of the fluid due to the presence of NPs at low concentrations [2,3,4]. Since the specific heat capacity (C_p) is one of the variables that measures the amount of heat that can be stored by a material, it is the property with highest interest for evaluating thermal energy storage (TES) systems. The reviewed literature shows exceptional C_p values with increments up to 30% when 1% in weight (wt.) of NPs are added to the base fluid [5].

According to this, in the last years NFs have become an interesting TES media to be implemented in concentrate solar power (CSP) plants [6,7] because the presence of NFs may improve the thermal properties of solar salt, used in these plants as TES media and HTF, which consists in the eutectic mixture of KNO_3 and $NaNO_3$ [5]. Obviously, the improvement of the base fluid's thermal properties would drive to a more efficient energy storage and consequently, to more efficient CSP plants [8] (e.g., higher thermal capacities would imply the volume reduction of the storage tanks [9]). Besides their use in solar energy applications [10,11], NFs are also being considered as heat transfer fluids [12], lubricants [13], in electronics [14], automotive [15,16], industrial cooling [17], nuclear systems [18], quantum dots [19] or in heating buildings [20,21].

Materials with these properties could significantly improve thermal storage efficiency. Although great advances have been made in this field, there is still a long way to do to fully understand the phenomenon that provokes the C_p enhancement [22]. Moreover, other factors as the influence of the size, concentration and density of nanoparticles, C_p of the base fluid or even the pH and temperature of the sample can have a great influence on the final properties [23]. Another drawback is the high dispersion observed in the published C_p values, under similar or in some cases, the same experimental conditions. Table 1 lists C_p variation, ΔC_p, for different solar salt-based NFs with 1 wt% of different NPs. ΔC_p corresponds to the difference in C_p of NFs and the $NaNO_3$-KNO_3 base

* Corresponding author.
E-mail address: ana_inesfernandez@ub.edu (A.I. Fernández).

https://doi.org/10.1016/j.molliq.2021.118316
0167-7322/

Table 1
Specific heat capacity variation, ΔC_p, of solar salt nanofluids with 1 wt% of nanoparticles with different sizes.

Base	Nanoparticle	Average Size (nm)	Average Temperature (°C)	ΔC_p (%)	References
$NaNO_3$– KNO_3 (60:40)	SiO_2	5	113.3,266.6,233.3	8,19,10	[27,50,51]
		7	183.3	0.8	[50,51]
		10	113.3, 233.3, 500	12,13,13	[50,27,52]
		12	223.3	25.03	[50,28]
		16	200, 250	8.9, 8.9	[50,52]
		102.5	40, 400	−0.34, 6.65	[52]
		20	200, 200, 350	17.6, −2, 17.6	[50,52]
		25	400	21.1, 20.3, 9.5, 10.6, 15.82	[53]
		30	266.6, 113.3, 233.3	25, 19, 21	[50,51,27]
		60	233.3, 113.3	28, 27	[50,27]
	Al_2O_3	13	183.3, 125, 125, 230	5.9, 19.9, 5.9, 3	[50,51,47,54]
		50	230	6	[54]
	SiO_2 - Al_2O_3	7	185, 272.5	28.9, 2.6	[52,29]
		41	396	30	[55]
		101	183.3, 125	22.5, 57.7	[50,51]
		103.5	185, 272.5	14.9, 0.8	[52,47]
	TiO_2	20	183.3, 125	−6.3, −6	[50,51]
		50	350, 182.5	−2.19, 1.6	[56]
	Al-Cu	160	300, 350, 400	0.07, −1.34, −3.69	[57]
	CuO	29	295	−1.27	[52,58]
		50	182.5, 350	6.3, −1.97	[56]
	Sn-Al_2O_3	180	80, 189, 280	0.62, 8.16, 3.99	[59]
	Sn-SiO_2	180	80	−1.26, 5.69, 5.88	[59]
	Fe_2O_3	30	350, 182.5	2.19, 9.1	[56]
	Sn	180	80, 180, 280	−5.09, 1.79, 2.02	[59]

fluid. A high dispersion of the ΔC_p is observed ranging from −5% to 22%. Moreover, different methodologies and techniques have been used to measure the C_p value (i.e., standard ASTM E1219[24], ASTM E2716[25] or the Areas Method[26]). In particular, the C_p values have been obtained by dissimilar number of samples and measurement repetitions. For example, B. Dudda et. al [27] or Z. Jiang et al. [28] in their studies measured up to 5 samples and 3 measurement repetitions. In opposite, M. Chieruzzi [29] obtained the C_p value by means of 1 sample and 6 measurement repetitions. Therefore, it is evident that there is a lack of a methodological procedure that makes impossible the direct comparison among results. Likewise, in the light of the ΔC_p values in Table 1, there is not a clear tendency about the effect of temperature in the nanofluids behaviour. Similar tendencies and inconsistencies have been found in other base fluids such as molten salts [30–33], water [34–37], ethylene and propylene glycol [38–42] or oils [39,43–45]. This fact points out that there is not a clear trend or specific values about NFs properties [46–49]. Thereby, the difficulties to obtain a representative sample is one of the possible reasons of these discrepancies. Obviously, this fact makes difficult to take a step forward in the NFs implementation and development for industrial applications.

This work aims at obtaining a statistically representative sampling of NFs to ensure accurate thermophysical results after their characterization. The study comprises the evaluation by means of differential scanning calorimetry (DSC) of thermophysical properties of NFs such as specific heat capacity, melting point and melting enthalpy, measuring a high number of samples. Sodium nitrate has been used as fluid along with three different NPs, silica (SiO_2), alumina (Al_2O_3), and montmorillonite (MMT). All the results have been compared with pure $NaNO_3$ used as a reference at the same experimental conditions. Furthermore, the chemical composition of the samples has been studied via an Inductively Coupled Plasma (ICP) analysis to determine the NP concentration, and to obtain a clear correlation between the NP concentration and the specific heat capacity variation. The statistical procedure used and the proposed methodology can contribute to the field in different ways; first, facilitating the comparison between results and, second, providing a clearer point of view about the thermophysical properties trends of NFs.

2. Experimental procedure and methodology

2.1. Sample preparation

The NFs were synthetized in our laboratories starting from sodium nitrate (Sigma Aldrich, 99.995%) as base fluid and then doped with three types of NPs: 5–15 nm diameter silica (Sigma Aldrich, 99.5%), 13 nm diameter alumina (Sigma Aldrich, 99.995%), and the clay montmorillonite (Nanomer® I.44P, Sigma-Aldrich) with a basal distance between 24 and 26 Å. To prepare the NF samples, a standard dissolution method [60] was followed (see Fig. 1).

1. To prepare 50 g sample (salt + NPs)
2. To dissolve the salt in 30 mL distilled water
3. To sonicate for 10 min for a correct dispersion of the NPs inside the salt
4. To dry the samples in an oven at 105 °C until the total water evaporation and recrystallization of the material
5. To grind the sample in an Agatha mortar

NFs can be synthesized by several methods, and all of them share the same objective of avoiding or reducing the agglomeration of NPs for thus, synthetizing a stable and durable NF. The methods reported in the literature use commercial NPs or synthetic ones although in such a case, they also report the description of the synthetic path.

Nanofluids can be prepared by means of two main paths, the one or the two-step method. In the one step method, the production of NPs and their dispersion are done simultaneously. On the contrary, the two-step method uses commercial or previously synthetized NPs. These paths include different methods such as dry mixing, dry milling, dissolution method, or magnetic stirring [61]. Furthermore, the literature suggests that the synthesis method has a strong influence on the NPs dispersion, and consequently, on the final thermophysical properties of the NFs [53,62,3]. While the influence of the synthesis method on the final properties is covered in the literature there is a lack of information about the reproducibility between different synthetized lots following the same methodology.

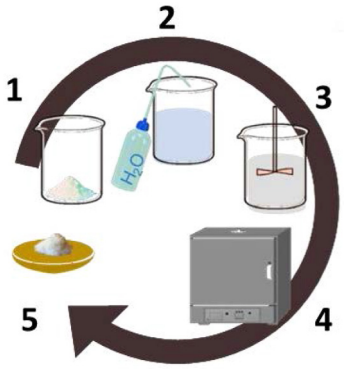

1. To prepare 50 g sample (salt + NPs)
2. To dissolve the salt in 30 mL distilled water
3. To sonicate for 10 minutes for a correct dispersion of the NPs inside the salt
4. To dry the samples in an oven at 105 ºC until the total water evaporation and recrystallization of the material
5. To grind the sample in an Agatha mortar

Fig. 1. 1-step nanofluid synthesis scheme.

2.2. Sampling procedure and measurement methodology recommendation

A standard quartering method was applied during the sampling [63]. Since the quantity of sample under study is small (≈ 50 g, see Section 2.1) , conventional quartering instruments are not useful. For that reason, an own riffle splitter (Fig. 2) suitable for small samples was designed in Autocad and printed on a Prusa i3, Anycubic 3D printer. Thus, the amount of sample required to be processed was around the amount analysed by the DSC equipment (≈ 10–15 mg) .

For each type of NF sample, three independent lots of 50 g were synthetized (see section 2.1.), and each lot was quartered in eight batches (sub-samples), obtaining 24 representative samples per NF. In the case of pure $NaNO_3$, the 3 lots were subdivided in four batches (12 samples). Therefore, a total amount of 84 samples were obtained. A schematic representation of the sampling procedure followed is depicted in Fig. 3. The thermophysical characterization of each sample was carried out in three steps; (1) thermal cycle from 25 °C to 450 °C for measuring the melting enthalpy and the melting temperature, (2) two consecutive measurement repetitions of C_p at 150 °C, 250 °C, 350 °C and 450 °C, and (3) repetition of the thermal cycle from 25 °C to 450 °C. The full process generated 384 measurements per type of NF and thermophysical property (i.e., 48 measurements for each property). Finally, all the values obtained were statistically analyzed.

2.3. Characterization

2.3.1. Thermophysical characterization

The melting temperature was characterized by three parameters: the onset temperature (T_{on}) when the sample starts the melting process, the peak temperature (T_{peak}) when the sample is half-melted and the endset temperature (T_{end}) when the sample finishes the melting process. Based on the literature, the reported average melting temperature, T_m, of pure $NaNO_3$ is 307 °C and the melting enthalpy value, ΔH_m, varies in the range 172–187 J g^{-1} [64]. Nonetheless, the recommended values obtained through differential scanning calorimetry (DSC) are T_m = 307 °C and ΔH_m = 178 J g^{-1} [65]. In this work, T_m, ΔH_m and C_p, have been analysed by Differential Scanning Calorimetry (DSC 822e from Mettler Toledo). All the measurements were performed at inert atmosphere, under a 50 mL/min N_2 constant flow. T_m and ΔH_m measurements were performed by a dynamic method from 25 °C to 450 °C, using a 0.5 K/min heating rate. The C_p values were measured at 150 °C, 250 °C, 350 °C and 450 °C, and determined through the areas method described by Ferrer et al. [26] which is a method more accurate than both dynamic and step methods. The amount of sample analysed was around 10 mg within a 100 μl pined aluminium crucible.

Notice that, two consecutive measurements of C_p were run for each sample and that, prior to the measurement each sample was introduced into the oven at 100 °C to avoid humidity in the samples due to the high hygroscopic nature of the species.

In addition, two measurements have been analysed namely first and second runs. This double run method applies because during the first measurement, the samples have undefined contact between the bottom of the crucible and the sample surface.

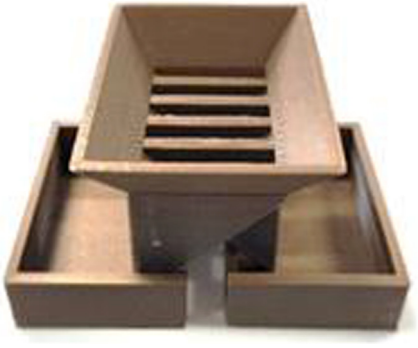

Fig. 2. Mini-riffle splitter system printing in 3D.

2.3.2. Chemical characterization

Inductively Coupled Plasma Atomic Emission Spectroscopy (-ICP-AES) analysis was performed with PerkinElmer ELAN 6000. These measurements were performed in order to determine the concentration of NPs in the samples previously analyzed by DSC. The samples were digested in 100 mg aliquots with 1 mL of HNO_3 and 1 mL of HF, and they were kept during 24 h in an oven at 90 °C. Finally, 25 mL deionized H_2O were added. This technique allows to analyze the Si and Al content of SiO_2, Al_2O_3 and MMT NPs.

2.3.3. Statistics

The statistical analysis of the obtained results was carried out via the independent-sample Student's *t*-test. This test allows discarding non-repeatable data among the entire population of results. The p-value is the probability that the results from the sample data occurred by chance and it ranges from 0 to 1. Thus, a p-value of 0.01 means there is only a 1% probability that the results from an experiment happened by chance. Low p-values are good, and they indicate that the data did not occur accidentally. In most cases, a p-value of 0.05 is accepted to mean the data is valid. In this study three p-values have been used, $p < 0.05$ (little significant differences), $p < 0.001$ (quite significant differences) and $p < 0.0001$ (highly significant differences).

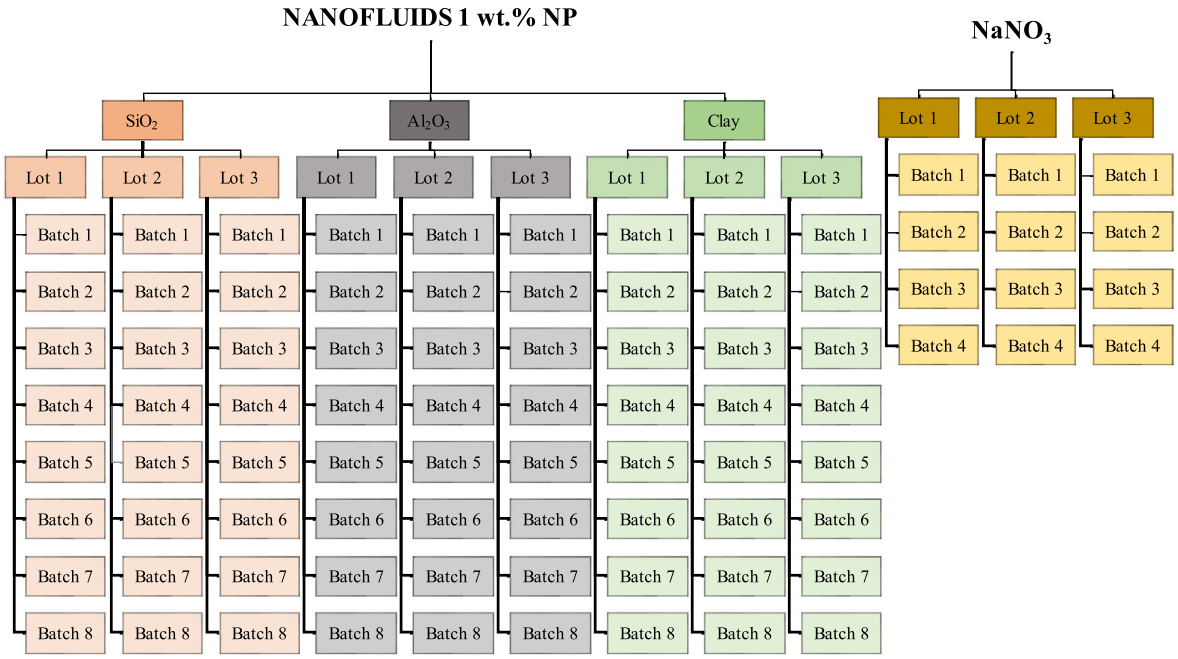

Fig. 3. Schematic representation of the quartering performed for all the samples of the three NFs and also for pure sodium nitrate: $NaNO_3$-1 wt% SiO_2 NPs (orange), $NaNO_3$-1 wt% Al_2O_3 NPs (grey), $NaNO_3$-1 wt% MMT NPs (green) and pure $NaNO_3$ (yellow).

Additionally, it was taken into account the uncertainty suggested by the DSC manufacturer, Mettler Toledo [66], described in Table 2.

Finally, the total standard deviation was calculated following the equation (1), taking into account the systematic error, equation (2), that considers the four sources of error listed in Table 2, and finally, the random error, equation (3), where σ is the standard deviation, p_c is the confidence level, N is the population size, x_i is the observed value of the sample items, and $\bar{x}$ is the mean value of these observations.

$$\sigma_{\text{total}} = \sqrt{(\sigma_{\text{sistematic}})^2 + (\sigma_{\text{random}})^2} \quad (1)$$

$$\sigma_{\text{sistematic}} = \sqrt{(0.2)^2 + (0.5)^2 + (1.5)^2 + (3)^2} = \mp 3.4\%(p_c = 68\%) \quad (2)$$

$$\sigma_{\text{random}} = \sqrt{\frac{1}{N-1}\hat{A} \cdot \sum_i (x_i - \bar{x})^2} \quad (3)$$

Table 2
Source and uncertainty of the DSC measurements.

Source	Measurement uncertainty
Mass of the test specimen	± 20 μg (e.g., reproducibility of the balance; if the mass is about 10 mg, this corresponds to ± 0.2%)
Put the sample into the crucible	negligible
Thermal contact with the crucible	± 0.5% (estimate)
Heating rate	negligible
Gas Flow	negligible, if adjusted under the same conditions
Adjustment	± 1.5% (uncertainty of the calibration material)
Integration limits	± 3% (statistics of repeated evaluations)
Baseline type	

3. Results and discussion

The results are presented using box-plot type distributions. Each set of results associated to a property is represented by a box. The box is formed by three horizontal lines; the bottom one that corresponds to the 25% of the results variance (i.e., first quartile, Q1), the upper one to the 75% of the results variance (i.e., third quartile, Q3) and the middle one that corresponds to the median, that is the 50% of the results variance (i.e., second quartile, Q2). Thus, the box itself represents the set of values associated to a variable but excluding the 25% of values furthest away from the median. Vertical lines represent the maximum and minimum values of the variable considering that the maximum value corresponds to 1.5 times the interquartile Q3–Q1 range. The values beyond these vertical lines correspond to atypical or outlier values also included in this study. Finally, the dots and squares inside the boxes represent the mean values [67,68].

3.1. Melting temperature

The values for the melting temperature of $NaNO_3$ are in good agreement with the values reported in the literature. Fig. 4 shows the box-plot distributions for the melting parameters of the three NFs derived from the DSC: T_{on} (red) that correspond to the intersection point between the baseline before the phase change process starts and the inflectional tangent , T_{peak} (blue) that corresponds to the temperature at the transformation peak, and T_{end} (green) that corresponds to the temperature when the transformation is completed. Moreover, the values for the melting temperature of pure $NaNO_3$ are also included in Fig. 4 (grey boxes) showing a good agreement with the reported value of T_m = 306.7 ± 0.2 °C [65].

As above-mentioned, for each sample two consecutive measurements (runs) were performed and analysed individually. During the first measurement no significant differences appear regarding the T_{on} of the pure $NaNO_3$. However, T_{peak} and T_{end} show increments on their values, suggesting a slower melting process.

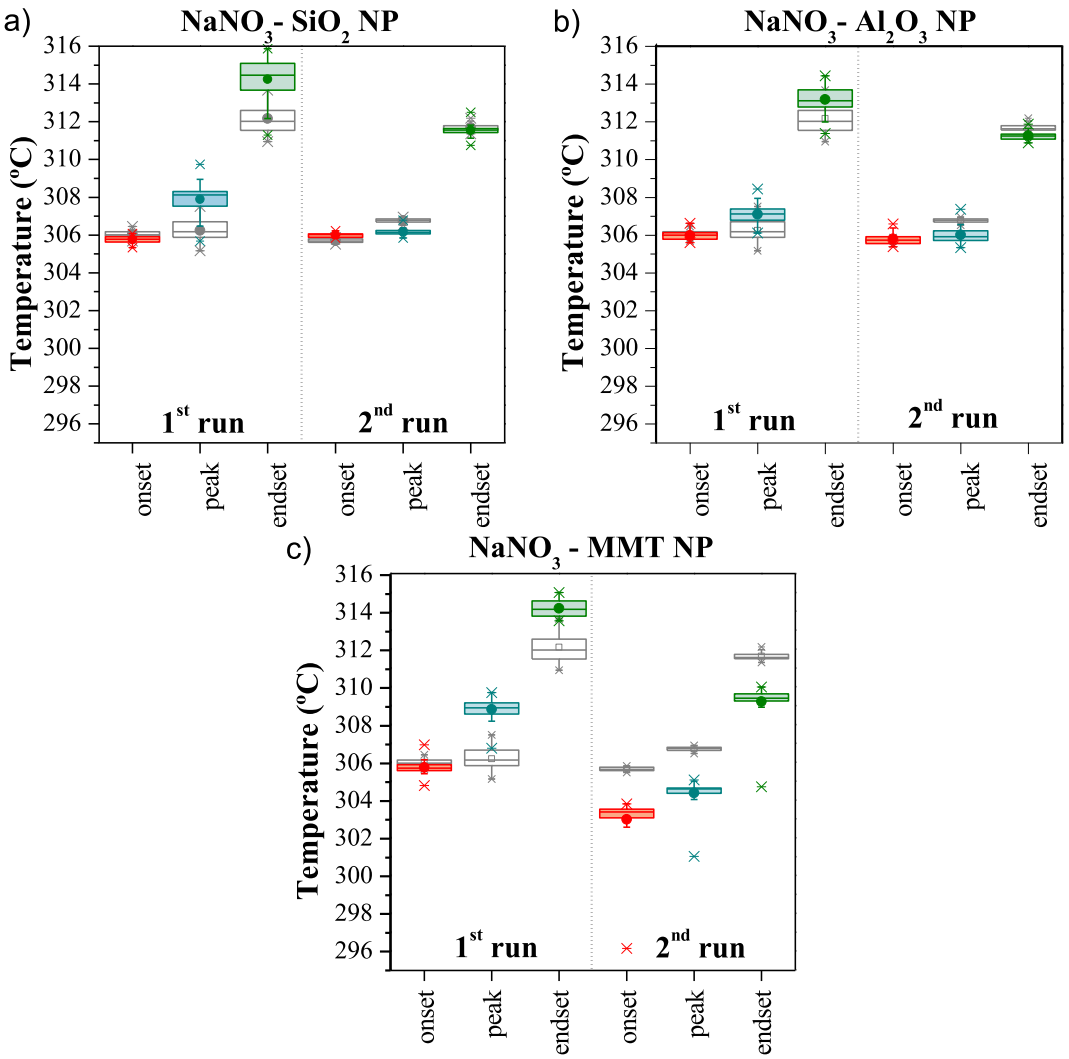

Fig. 4. Box-plot of the melting point values of the NFs over a population of N = 24. Onset, endset and peak temperature correspond to orange, green and blue boxes, respectively. The results obtained during the first melting run (left) and at the second melting run (right) are also shown: a) $NaNO_3$- 1% wt. SiO_2 NFs, b) $NaNO_3$- 1% wt. Al_2O_3 NFs and c) $NaNO_3$-1% wt. MMT NFs. Grey boxes stand for pure $NaNO_3$ with a statistical sampling of N = 12.

These differences mainly are due to the effect of the particle size of the $NaNO_3$ samples. Therefore, to avoid this effect and guarantee the good quality measurement of the thermophysical properties, the first run is absolutely necessary to ensure that the crucible bottom base is completely filled[69]. Indeed, for all the samples (pure $NaNO_3$ and NFs) the values of the second run were less dispersed and more homogeneous (minor interquartile range, Q1–Q3) than during the first measurement, particularly considering the T_{peak} and the T_{end}.

$NaNO_3$ based NFs with SiO_2 and Al_2O_3, Fig. 4-a and Fig. 4-b, respectively, shows a similar T_{on} behaviour than $NaNO_3$ pure salt with no significant differences ($p > 0.05$) (run 2). On the contrary, the MMT nanofluid shows highly significant differences ($p < 0.0001$) on the T_{on}, Fig. 4-c. Then, only MMT NPs change the $NaNO_3$ T_{on} (beginning of the melting process).

In general, these trends are not in agreement with already reported data. For example, the results from M. Chieruzzi et al., indicate that T_{on} decreases up to 9.7 °C adding NPs of SiO_2, Al_2O_3 and SiO_2/Al_2O_3 into solar salt [29,70]. Likewise, other studies with the addition of other kind of NPs in molten salts like CuO, TiO_2 or Fe_2O_3, show a similar T_{on} drop [71,56].

On the other hand, for both Al_2O_3 and MMT NFs (run 2), a slight shift in the T_{peak} was observed, with highly significant differences ($p < 0.0001$) in front of the pure $NaNO_3$ (i.e., $T_{peak} < 1$ °C and $T_{peak} > 2$ °C, respectively). On the contrary, for SiO_2 NFs (Fig. 4-a) there are not significant differences for T_{peak} ($p > 0.05$).

A similar tendency was found in the value of T_{end}; the addition of NPs decreases the endset temperature (i.e., $T_{end} < 1$ °C and $T_{end} < 2$ °C for Al_2O_3 and MMT NFs, respectively). On the contrary, for SiO_2 NFs no significant differences were found ($p > 0.05$). Therefore, with Al_2O_3 and MMT NPs the phase change transformation is completed at lower temperatures. Furthermore, the obtained results show a reduction of the three melting temperatures when adding MMT NPs. This fact agrees with the results obtained by Q. Xie et al. [48] for who the addition of graphene nanoplatelets into solar salts exhibited a reduction of the three temperatures.

It is important to highlight the outlier values in MMT NFs at the second run for the three parameters, (Fig. 4-c) that represent an anomalous data, suggesting a possible measurement error or abnormal behaviour of the sample, as suggested in a previous work[22].

Nonetheless, no important changes were found in the melting performance of the NFs. Notice that the mean values and the standard deviations from Fig. 4 are listed in Table 3.

3.2. Melting enthalpy

The same statistical treatment was performed for the melting enthalpy (ΔH_m) of the three NFs (Fig. 5). As in the case of the melting temperatures, there are differences between the two thermal cycles (runs).

For the first run, the ΔH_m was higher (up to 6%) than in the second run, and this behaviour is observed for all NFs under study as well as for the pure $NaNO_3$. In all the cases, during the second run, the mean ΔH_m values decrease up to 7%, nonetheless without statistically significant differences ($p > 0.05$). As in the melting temperature, this is mainly due to grain size effects of the sample [69]. However, only for Al_2O_3 NFs (Fig. 5-b), the ΔH_m decreases with slight significant differences ($p < 0.05$).

Therefore, non-important modification in the latent heat of fusion is obtained with the addition of 1 wt% of NPs into $NaNO_3$ pure salt. Notice that the outliers for the MMT NFs (Fig. 5-c) correspond to the same outlier samples obtained in the melting temperature measurements (Fig. 4-c). Nevertheless, previous results show different behaviours; thus, M. Lasfargues et al. [72], and Y. Luo et al. [71] determined a decrease in ΔH_m adding 1 wt%. CuO and TiO_2 NPs in molten salts, whereas Y. Li et al. [73], and A. Awad et al. [56] obtained an enhancement of ΔH_m with the incorporation of SiO_2, Fe_2O_3, CuO and TiO_2 NPs also in molten salts, in agreement with our results. Otherwise, G. Qiao et al. [74], and P. Myers et al. [75] stated non-significant modifications for the ΔH_m values when SiO_2 or CuO NPs are added into the salt.

Indeed, it is remarkable that all the cited studies, generally, did not use more than three different samples for the measurement of the thermophysical properties. In addition, these previous works sometimes carried out up to five repetition measurements of the same sample and discarded the first run measurement. Based on the previous results we are confident that the methodology described herein reduces the error associated to the ΔH_m determination.

3.3. Specific heat capacity- synthesis method

The C_p analysis among different synthesized lots with identical preparation was performed to analyse the statistical error due to the synthesis procedure. C_p values as a function of temperature are shown in Fig. 6. The C_p results show an increase with temperature, from approximately 0.8 J g^{-1} K^{-1} up to 1.3 J g^{-1} K^{-1}. Statistical p-value analysis shows a slight significant difference between the lots of the three formulated NFs.

Thereby, the C_p of the SiO_2 NFs shown in Fig. 6-a, has significant differences ($p < 0.05$) when it is measured at 100 °C between lots 1–3 and 2–3. The same is observed between lots 1–3 at 200 °C, and lots 1–2 at 350 °C ($p < 0.05$). In the case of the Al_2O_3 NFs C_p (Fig. 6-b), there is only a significant difference ($p < 0.05$) between lots 2–3 at 350 °C. Finally, in the case of MMT NFs (Fig. 6-c), a slight significant difference between lots 1–3 ($p < 0.05$) is observed.

Therefore, these results highlight that to determine a more precise C_p value, the systematic error associated to the NFs preparation needs to be considered. Accordingly, to determine more precisely the C_p, it is mandatory to average samples from different lots. On the other hand, it is important to highlight that there are differences between lots when these samples are measured at different temperatures, and this fact does not correlate for all the temperature ranked. This effect evidences the presence of uncontrolled physicochemical phenomena that take place at different temperatures.

3.4. Specific heat capacity of NFs

Fig. 7 shows the C_p mean values obtained from all the analysed NF samples. The C_p values as a function of temperature for the three NFs and for the pure $NaNO_3$ are plotted in Fig. 7-a. The obtained C_p values for the pure $NaNO_3$ at 100 °C, 200 °C, 350 °C and 450 °C are 0.66 ± 0.07 J g^{-1} K^{-1}, 0.85 ± 0.07 J g^{-1} K^{-1}, 1.13 ± 0.09 J g^{-1} K^{-1} and 1.17 ± 0.08 J g^{-1} K^{-1}, respectively. These values are lower than those reported by T. Bauer et al. [76] which correspond to 1.25 J·g^{-1}·K^{-1} at 100 °C, 1.55 J g^{-1} K^{-1} at 200 °C, and around 1.65 J g^{-1} K^{-1} once the samples are at the liquid state.

This deviation of the C_p can be caused both by the presence of impurities in the salt and by the low amount of mass analyzed in the DSC, as demonstrated by B. Muñoz-Sánchez et al. [77]. In solid state (T < 307 °C) the three NFs improved their C_p in comparison of the pure $NaNO_3$, with significant statistical differences ($p < 0.0001$). Nevertheless, the differences were minor at the liquid state (T > 307 °C).

For the case of SiO_2 and MMT NFs no statistical differences were found between the NF and the pure $NaNO_3$ ($p > 0.05$) at 450 °C. Only in the case of adding Al_2O_3 NPs to the salt derives in a C_p enhancement in liquid state with slight significant differences ($p < 0.05$). Additionally, Fig. 7-b depicts the C_p variation in front of the pure $NaNO_3$ with the temperature. It can be seen that the mean values of the C_p variation of the three NFs decay with increasing the temperature (i.e., up to 34% in the case of MMT NFs, 30% for Al_2O_3 NFs and 27% for SiO_2 NFs, from 100 to 450 °C) and they tend to even lower values at 450 °C (i.e., −2% for SiO_2 NFs, 3% for MMT NFs and 12% for Al_2O_3 NFs). It is noticeable the high standard deviation for all the values of the three NFs.

Fig. 8 shows the C_p variation in a box-plot graph from 100 °C to 450 °C. Firstly, it can be observed that the C_p values for each NF show a high variability at 100 °C evidenced by the difference between Q1 and Q3 quartiles, more evident in the case of Al_2O_3 (Fig. 8-b) and MMT NFs (Fig. 8-c). Similar trends are observed at higher temperatures with C_p values with positive and negative variations (high dispersion) although the C_p variation decreases with temperature while the NFs are solids (T < 307 °C). Once the NFs melted the C_p variation corresponding to the liquid state remains approximately constant (T > 307 °C). However, the high dispersion observed in the C_p values agrees with the opposing

Table 3
Mean values and standard deviations of the melting parameters; onset, peak, and endset temperatures, for pure $NaNO_3$ and the three $NaNO_3$ based nanofluids with 1% wt. of SiO_2, $Al2O_3$ and MMT nanoparticles, during the first and second melting measurements.

System	Cycle	onset (°C)	(±)	peak (°C)	(±)	endset (°C)	(±)
$NaNO_3$	Run 1	306.0	0.2	306.2	0.8	312.2	0.8
	Run 2	**305.7**	**0.1**	**306.7**	**0.2**	**311.7**	**0.3**
$NaNO_3$-SiO_2	Run 1	305.7	0.2	308.1	0.9	314.4	1.2
	Run 2	**306.0**	**0.1**	**306.1**	**0.2**	**311.5**	**0.3**
$NaNO_3$-Al_2O_3	Run 1	305.9	0.3	307.1	0.6	313.0	0.8
	Run 2	**305.7**	**0.3**	**306.0**	**0.4**	**311.2**	**0.2**
$NaNO_3$-MMT	Run 1	305.7	0.4	308.8	0.6	314.2	0.5
	Run 2	**303.0**	**1.5**	**304.5**	**0.9**	**309.3**	**1.0**

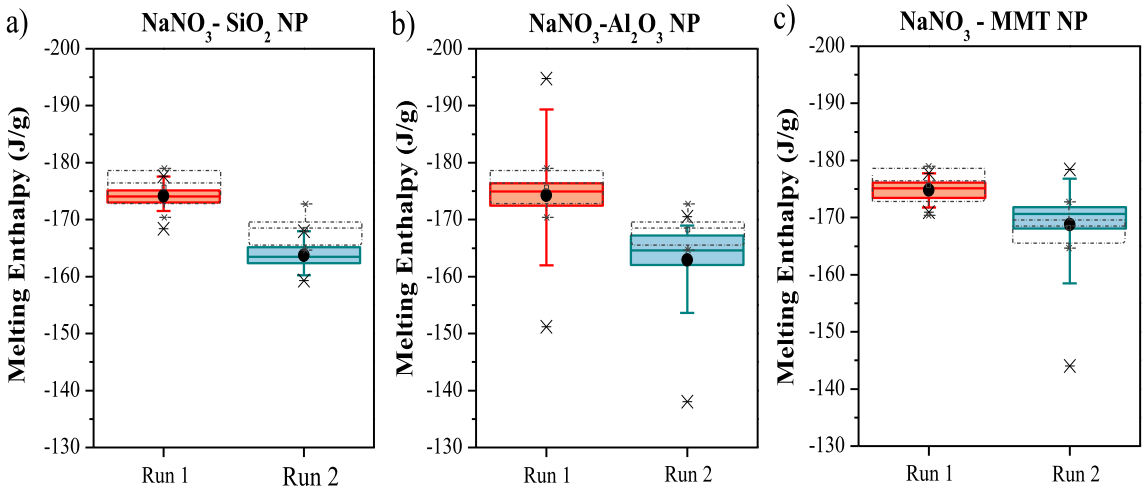

Fig. 5. Box-plot of the melting enthalpy values of the NFs over a population of N = 24. The results obtained during the first melting run (orange) and at the second melting run (blue) are also shown: a) $NaNO_3$- 1% wt. SiO_2 NFs, b) $NaNO_3$- 1% wt. Al_2O_3 NFs and c) $NaNO_3$-1% wt. MMT NFs. Grey dotted lines represent the statistical value of pure $NaNO_3$ with a statistical sampling of N = 12.

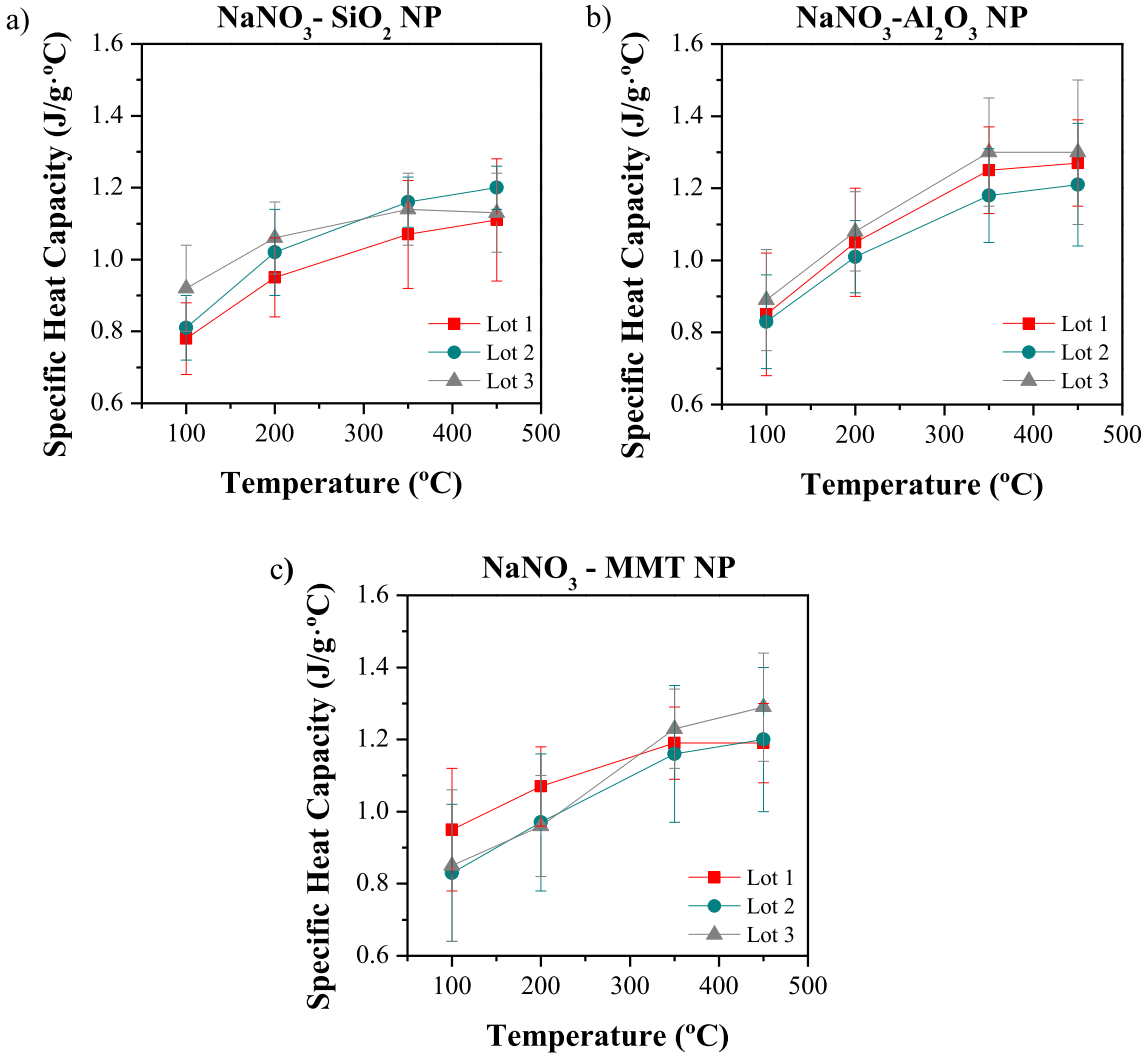

Fig. 6. Specific heat capacity of the NFs at selected temperatures in the range 100 °C to 450 °C for the three independent synthetized lots with a statistical sampling of N = 8 each lot. a) $NaNO_3$- 1% wt. SiO_2 NFs, b) $NaNO_3$- 1% wt. Al_2O_3 NFs and c) $NaNO_3$-1% wt. MMT NFs. Lots 1, 2 and 3 are represented by squares, circles and triangles, respectively.

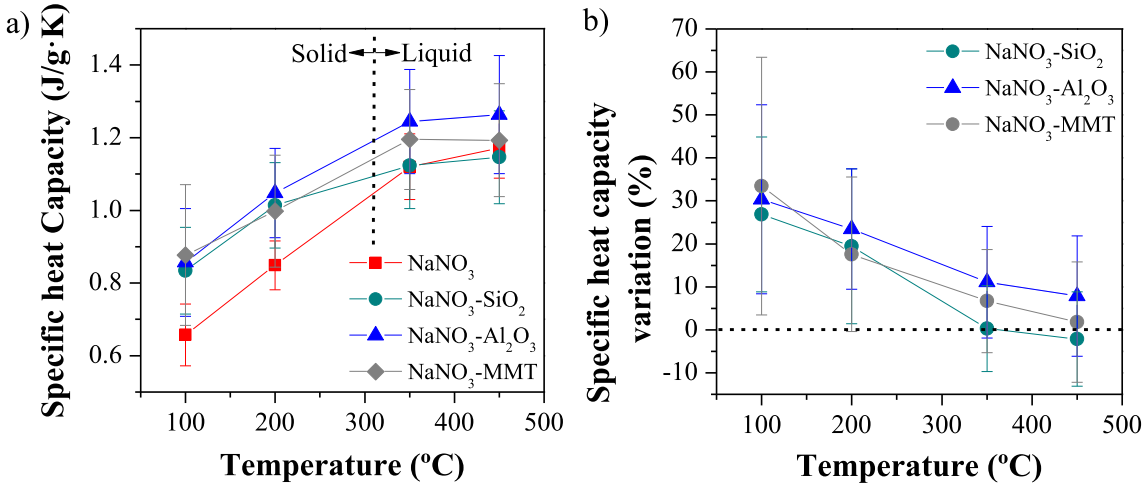

Fig. 7. a) Specific heat capacity mean values and b) specific heat capacity variation of the NFs at selected temperatures in the range 100 °C to 450 °C for a statistical sampling of N = 48 for $NaNO_3$- 1% wt. SiO_2 NFs (circle), $NaNO_3$- 1% wt. Al_2O_3 NFs (triangle), $NaNO_3$-1% wt. MMT NFs (rhombohedral) and pure $NaNO_3$ (squares) with only N = 24 measurements. Lots 1, 2 and 3 are represented by squares, circles, and triangles, respectively.

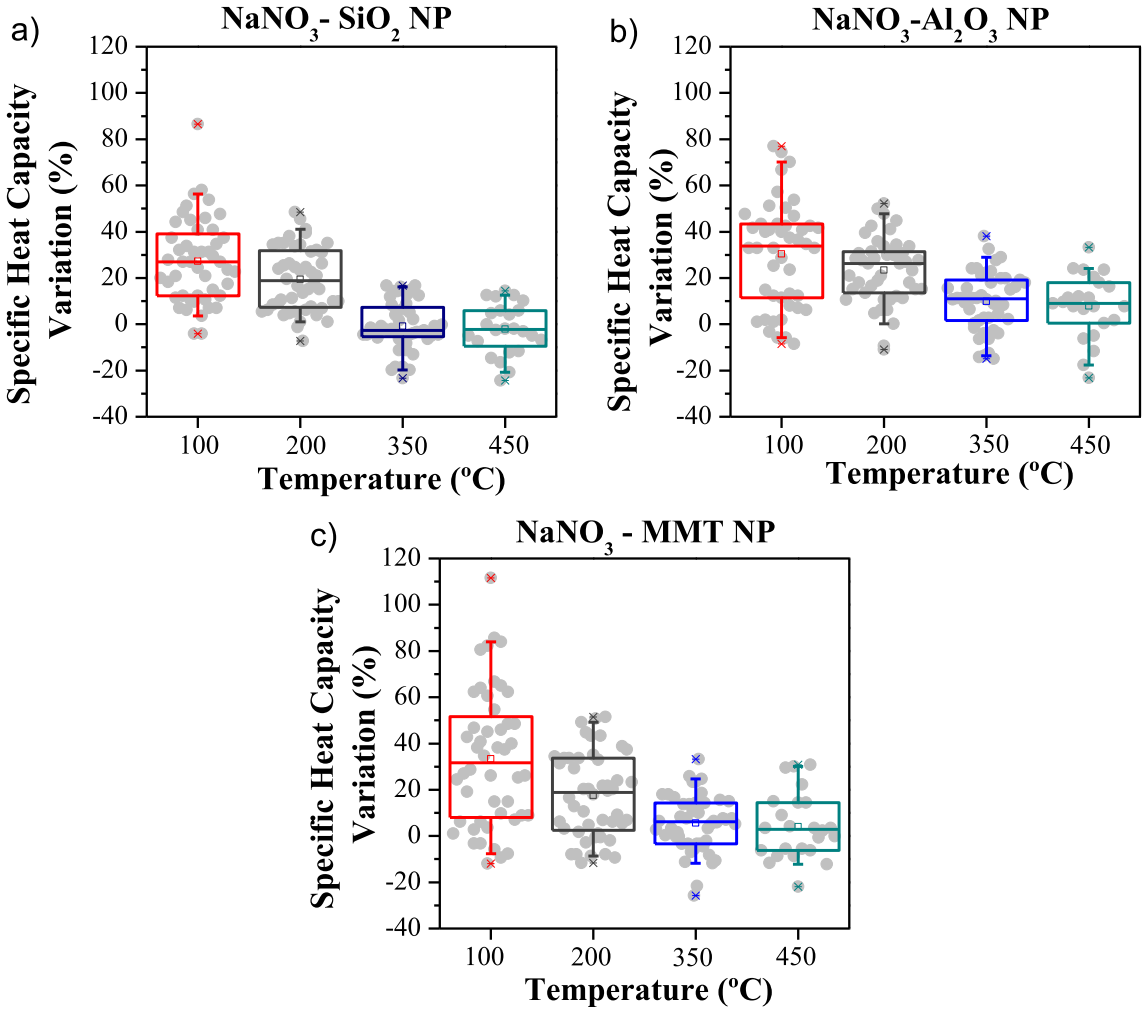

Fig. 8. Box-plot of the specific heat variation of the NFs at selected temperatures in the range 100 °C to 450 °C, over a population of N = 12. a) $NaNO_3$- 1% wt. SiO_2 NFs, b) $NaNO_3$- 1% wt. Al_2O_3 NFs and c) $NaNO_3$-1% wt. MMT NFs. Grey dots represent all the samples analysed per NF and temperature.

results already published [50,52,78–80] that show enhancements and decrements of C_p values for the same NF system.

One possible explanation to the high dispersion observed is the difficulty to obtain a representative NF sample because when a NF is sampled, the samples under study probably have different concentrations of NP in their compositions.

For that reason, it is mandatory to perform a sample composition characterization in order to monitor the real NP wt% content

Table 4
Nanoparticle concentration obtained by ICP measurements for two samples of three independent synthetized lots of $NaNO_3$- 1% wt. SiO_2 NFs, $NaNO_3$- 1% wt. Al_2O_3 NFs and $NaNO_3$- 1% wt. MMT NFs.

System	Lot 1	Lot 2	Lot 3
	% wt.		
$NaNO_3$- SiO_2	0.71	0.75	0.66
	0.68	0.64	0.66
$NaNO_3$-Al_2O_3	0.86	0.87	0.83
	0.77	1.04	0.89
$NaNO_3$-MMT	0.45	0.45	0.48
	0.48	0.55	0.48

of each sample to ensure the proper sampling procedure along with the reproducibility.

Table 4 shows two repetitions of the ICP-AES measurements for each NF lot. In general, the concentration obtained is lower than the expected (1 wt%). Only one sample, Al_2O_3 NF lot 2, has 1 wt% NPs concentration. This fact indicates a low NP dispersion within the salt and/or NP agglomeration, or the loss of NPs during the NF synthesis procedure.

Consequently, a complementary characterization using ICP-AES is required to better describe the properties of NFs, and to be able to compare results under the same conditions.

On the other hand, there are not specific correlations between the slight differences of the NPs concentration and the C_p variation. The obtained results for each sub-sample from the synthetized lots, suggest that an additional phenomenon occurs in the thermal properties (i.e., thermal interfaces or layering phenomenon [5,22,81]). Therefore, based on these results, to determine the main C_p variation, the conventional DSC methodology may not be the most accurate method to understand the NFs performance. For this reason, more experiments are necessary to understand the mechanisms occurring in the NFs and their precise characterization.

4. Conclusions

A sampling study of ionic nanofluids with a wide sampling collection (84 samples) was performed. The nanofluids were based on $NaNO_3$ salt as a base fluid with three kinds of nanoparticles: SiO_2, Al_2O_3 and montmorillonite (MMT) at 1% weight. The methodology used has allowed to measure enthalpy, melting temperature and C_p values and to obtain a reliable data collection.

The specific heat capacity decreases with temperature and is the property most influenced by the presence of nanoparticles, with variations between 80% and −20%. Furthermore, the nature of the nanoparticles showed an impact on the melting temperature behaviour with a slight decrease of the melting temperature in Al_2O_3 and MMT NPs. Despite of this, in the case of melting enthalpy, no significant differences were found by the addition of nanoparticles.

This study demonstrates the relevance of sampling for the evaluation of nanofluids and summarize some recommendations to present proper thermophysical values. The procedure proposed can be resumed in the following steps; (1) to obtain at least 2 independently synthesized samples, (2) from each independent sample, to obtain at least 3 sub-samples, (3) for each sub-sample perform at least 2 measurement repetitions (with the sample previously melted) and finally, (4) to perform statistical data treatment. This methodology is intended to facilitate the comparison between results and to obtain a representative value of the thermophysical properties of nanofluids.

According to this point, the significant differences regarding the Cp values after the sampling process can be explained due to the possible unsuitability of the DSC methodology to be used for measuring thermophysical properties of NFs. This statistical treatment opens the door to explain the high dispersion of the results regarding the Cp in the literature. Nonetheless, further experiments are needed to deeply understand the mechanisms behind nanofluids for their correct characterization.

CRediT authorship contribution statement

A. Svobodova-Sedlackova: Conceptualization, Data curation, Investigation, Methodology, Visualization, Writing – original draft. **C. Barreneche:** Methodology, Writing – review & editing. **P. Gamallo:** Funding acquisition, Supervision, Writing – review & editing. **A. Inés Fernández:** Conceptualization, Funding acquisition, Methodology, Writing – review & editing.

Declaration of Competing Interest

The authors declare that they have no known competing financial interests or personal relationships that could have appeared to influence the work reported in this paper.

Acknowledgments

This work was partially funded by the Spanish Ministry of Science, Innovation and Universities with projects RTI2018-093849-B-C32, RTI2018-094757-B-I00 (MCIU/AEI/FEDER) and MDM-2017-0767. The authors would like to thank also the Catalan Government for the quality accreditation given to their research group (DIOPMA 2017 SGR 0118 and 2017 SGR 13). DIOPMA is certified agent TECNIO in the category of technology developers from the Government of Catalonia. A.S thanks to Generalitat de Catalunya, AGAUR, for her Grant FI-DGR 2018.

References

[1] S. U. S. Choi, "Enhancing thermal conductivity of fluids with nanoparticles," *Am. Soc. Mech. Eng. Fluids Eng. Div. FED*, vol. 231, no. January 1995, pp. 99–105, 1995.
[2] M. Awais, A.A. Bhuiyan, S. Salehin, M.M. Ehsan, B. Khan, M.H. Rahman, Synthesis, heat transport mechanisms and thermophysical properties of nanofluids: A critical overview, Int. J. Thermofluids 10 (2021) 100086, https://doi.org/10.1016/j.ijft.2021.100086.
[3] S.A. Angayarkanni, J. Philip, Review on thermal properties of nanofluids: Recent developments, Adv. Colloid Interface Sci. 225 (2015) 146–176, https://doi.org/10.1016/j.cis.2015.08.014.
[4] A.G.N. Sofiah, M. Samykano, A.K. Pandey, K. Kadirgama, K. Sharma, R. Saidur, Immense impact from small particles: Review on stability and thermophysical properties of nanofluids, Sustain. Energy Technol. Assessments 48 (5) (2021), https://doi.org/10.1016/j.seta.2021.101635 101635.
[5] A. Svobodova-Sedlackova, C. Barreneche, G. Alonso, A.I. Fernandez, P. Gamallo, Effect of nanoparticles in molten salts – MD simulations and experimental study, Renew. Energy 152 (2020) 208–216, https://doi.org/10.1016/j.renene.2020.01.046.
[6] K. Khanafer, K. Vafai, A review on the applications of nanofluids in solar energy field, Renew. Energy 123 (2018) 398–406, https://doi.org/10.1016/j.renene.2018.01.097.
[7] T. Singh, M.A.A. Hussien, T. Al-Ansari, K. Saoud, G. McKay, Critical review of solar thermal resources in GCC and application of nanofluids for development of efficient and cost effective CSP technologies, Renew. Sustain. Energy Rev. 91 (February) (2018) 708–719, https://doi.org/10.1016/j.rser.2018.03.050.
[8] A. Alirezaie, M.H. Hajmohammad, A. Alipour, Do nanofluids affect the future of heat transfer?"A benchmark study on the efficiency of nanofluids&quot, Energy 157 (2018), https://doi.org/10.1016/J.ENERGY.2018.05.060.
[9] A. Alashkar, M. Gadalla, Thermo-economic analysis of an integrated solar power generation system using nanofluids, Appl. Energy 191 (2017) 469–491, https://doi.org/10.1016/j.apenergy.2017.01.084.
[10] H.A. Mohammed, H.B. Vuthaluru, S. Liu, Thermohydraulic and thermodynamics performance of hybrid nanofluids based parabolic trough solar collector equipped with wavy promoters, Renew. Energy 182 (2022) 401–426, https://doi.org/10.1016/j.renene.2021.09.096.
[11] Z. Said, A.A. Hachicha, S. Aberoumand, B.A.A. Yousef, E.T. Sayed, E. Bellos, Recent advances on nanofluids for low to medium temperature solar collectors: energy, exergy, economic analysis and environmental impact, Prog. Energy Combust. Sci. 84 (2021) 100898, https://doi.org/10.1016/j.pecs.2020.100898.

[12] H.R. Allahyar, F. Hormozi, B. ZareNezhad, Experimental investigation on the thermal performance of a coiled heat exchanger using a new hybrid nanofluid, Exp. Therm. Fluid Sci. 76 (2016) 324–329, https://doi.org/10.1016/j.expthermflusci.2016.03.027.
[13] X. Han, S.J. Thrush, Z. Zhang, G.C. Barber, H. Qu, Tribological characterization of ZnO nanofluids as fastener lubricants, Wear 468–469 (Dec 2021) 203592, https://doi.org/10.1016/j.wear.2020.203592.
[14] K.R. Aglawe, R.K. Yadav, S.B. Thool, Preparation, applications and challenges of nanofluids in electronic cooling: A systematic review, Mater. Today Proc. 43 (2020) 366–372, https://doi.org/10.1016/j.matpr.2020.11.679.
[15] M.B. Bigdeli, M. Fasano, A. Cardellini, E. Chiavazzo, P. Asinari, A review on the heat and mass transfer phenomena in nanofluid coolants with special focus on automotive applications, Renew. Sustain. Energy Rev. 60 (2016) 1615–1633, https://doi.org/10.1016/j.rser.2016.03.027.
[16] V. Delavari, S.H. Hashemabadi, CFD simulation of heat transfer enhancement of Al2O 3/water and Al2O3/ethylene glycol nanofluids in a car radiator, Appl. Therm. Eng. 73 (1) (2014) 380–390, https://doi.org/10.1016/j.applthermaleng.2014.07.061.
[17] A. Siricharoenpanich, S. Wiriyasart, P. Naphon, "Study on the thermal dissipation performance of GPU cooling system with nanofluid as coolant", *Case Stud*, Therm. Eng. 25 (April 2021) 100904, https://doi.org/10.1016/j.csite.2021.100904.
[18] V. Ghazanfari, M. Talebi, J. Khorsandi, R. Abdolahi, Thermal-hydraulic modeling of water/Al2O3 nanofluid as the coolant in annular fuels for a typical VVER-1000 core, Prog. Nucl. Energy 87 (2016) 67–73, https://doi.org/10.1016/j.pnucene.2015.11.008.
[19] M. Jamshidmofid, A. Abbassi, M. Bahiraei, Efficacy of a novel graphene quantum dots nanofluid in a microchannel heat exchanger, Appl. Therm. Eng. 189 (September) (2021) 116673, https://doi.org/10.1016/j.applthermaleng.2021.116673.
[20] D.P. Kulkarni, D.K. Das, R.S. Vajjha, Application of nanofluids in heating buildings and reducing pollution, Appl. Energy 86 (12) (2009) 2566–2573, https://doi.org/10.1016/j.apenergy.2009.03.021.
[21] Y. Cao, S.M. Seyed Alizadeh, M.T. Fouladvand, A. Khan, A. Taghvaie Nakhjiri, Z. Heidari, R. Pelalak, T.A. Kurniawan, A.B. Albadarin, Mathematical modeling and numerical simulation of CO2 capture using MDEA-based nanofluids in nanostructure membranes, Process Saf. Environ. Prot. 148 (2021) 1377–1385, https://doi.org/10.1016/j.psep.2021.03.007.
[22] A. Svobodova-Sedlackova, A. Calderón, C. Barreneche, P. Gamallo, A.I. Fernández, Understanding the abnormal thermal behavior of nanofluids through infrared thermography and thermo - physical characterization, Sci. Rep. 0123456789 (2021) 1–10, https://doi.org/10.1038/s41598-021-84292-9.
[23] M. Jamei, M. Karbasi, I. Adewale, M. Mosharaf-dehkordi, Specific heat capacity of molten salt-based nanofluids in solar thermal applications : A paradigm of two modern ensemble machine learning methods, J. Mol. Liq. 335 (2021), https://doi.org/10.1016/j.molliq.2021.116434 116434.
[24] ASTM E1269-11(2018), Standard Test Method for Determining Specific Heat Capacity by Differential Scanning Calorimetry. West Conshohocken,PA,www.astm.org, 2018
[25] ASTM International, ASTM E2716, Standard Test Method for Determining Specific Heat Capacity by Sinusoidal Modulated Temperature Differential Scanning Calorimetry, PA, www.astm.org, West Conshohocken, 2014.
[26] G. Ferrer, C. Barreneche, A. Solé, I. Martorell, L.F. Cabeza, New proposed methodology for specific heat capacity determination of materials for thermal energy storage (TES) by DSC, J. Energy Storage 11 (2017) 1–6, https://doi.org/10.1016/j.est.2017.02.002.
[27] B. Dudda, D. Shin, Effect of nanoparticle dispersion on specific heat capacity of a binary nitrate salt eutectic for concentrated solar power applications, Int. J. Therm. Sci. 69 (2013) 37–42, https://doi.org/10.1016/j.ijthermalsci.2013.02.003.
[28] H.Y. Ryu, Large enhancement of light extraction efficiency in AlGaN-based nanorod ultraviolet light-emitting diode structures, Nanoscale Res. Lett. 9 (1) (2014) 1–7, https://doi.org/10.1186/1556-276X-9-58.
[29] M. Chieruzzi, G.F. Cerritelli, A. Miliozzi, J.M. Kenny, L. Torre, Heat capacity of nanofluids for solar energy storage produced by dispersing oxide nanoparticles in nitrate salt mixture directly at high temperature, Sol. Energy Mater. Sol. Cells 167 (Dec 2017) 60–69, https://doi.org/10.1016/j.solmat.2017.04.011.
[30] H. Tian et al., Enhanced specific heat capacity of binary chloride salt by dissolving magnesium for higherature thermal energy storage and transfer, J. Mater. Chem. A 5 (28) (2017) 14811–14818, https://doi.org/10.1039/c7ta04169a.
[31] D. Shin, D. Banerjee, Enhancement of specific heat capacity of high-temperature silica-nanofluids synthesized in alkali chloride salt eutectics for solar thermal-energy storage applications, Int. J. Heat Mass Transf. 54 (5–6) (2011) 1064–1070, https://doi.org/10.1016/j.ijheatmasstransfer.2010.11.017.
[32] L.-d. Zhang, X. Chen, Y.-t. Wu, Y.-w. Lu, C.-f. Ma, Effect of nanoparticle dispersion on enhancing the specific heat capacity of quaternary nitrate for solar thermal energy storage application, Sol. Energy Mater. Sol. Cells 157 (2016) 808–813, https://doi.org/10.1016/j.solmat.2016.07.046.
[33] M.X. Ho, C. Pan, Optimal concentration of alumina nanoparticles in molten hitec salt to maximize its specific heat capacity, Int. J. Heat Mass Transf. 70 (2014) 174–184, https://doi.org/10.1016/j.ijheatmasstransfer.2013.10.078.
[34] C. Selvam, D. Mohan Lal, S. Harish, Thermal conductivity and specific heat capacity of water–ethylene glycol mixture-based nanofluids with graphene nanoplatelets, J. Therm. Anal. Calorim. 129 (2) (2017) 947–955, https://doi.org/10.1007/s10973-017-6276-6.
[35] C.J. Ho, J.B. Huang, P.S. Tsai, Y.M. Yang, Water-based suspensions of Al2O3 nanoparticles and MEPCM particles on convection effectiveness in a circular tube, Int. J. Therm. Sci. 50 (5) (2011) 736–748, https://doi.org/10.1016/j.ijthermalsci.2010.11.015.
[36] J. Choi, Y. Zhang, Numerical simulation of laminar forced convection heat transfer of Al 2O 3-water nanofluid in a pipe with return bend, Int. J. Therm. Sci. 55 (2012) 90–102, https://doi.org/10.1016/j.ijthermalsci.2011.12.017.
[37] V. Leela Vinodhan, K.S. Suganthi, K.S. Rajan, Convective heat transfer performance of CuO-water nanofluids in U-shaped minitube: Potential for improved energy recovery, Energy Convers. Manag. 118 (2016) 415–425, https://doi.org/10.1016/j.enconman.2016.04.017.
[38] S. Akilu, A.T. Baheta, A.A. Minea, K.V. Sharma, Rheology and thermal conductivity of non-porous silica (SiO2) in viscous glycerol and ethylene glycol based nanofluids, Int. Commun. Heat Mass Transf. 88 (Oct 2017) 245–253, https://doi.org/10.1016/j.icheatmasstransfer.2017.08.001.
[39] S.M.S. Murshed, Simultaneous measurement of thermal conductivity, thermal diffusivity, and specific heat of nanofluids, Heat Transf. Eng. 33 (8) (2012) 722–731, https://doi.org/10.1080/01457632.2011.635986.
[40] S.M.S. Murshed, Determination of effective specific heat of nanofluids, J. Exp. Nanosci. 6 (5) (2011) 539–546, https://doi.org/10.1080/17458080.2010.498838.
[41] A.K. Starace, J.C. Gomez, J. Wang, S. Pradhan, G.C. Glatzmaier, Nanofluid heat capacities, J. Appl. Phys. 110 (12) (2011) 124323, https://doi.org/10.1063/1.3672685.
[42] J.P. Vallejo, L. Ansia, J. Fal, J. Traciak, L. Lugo, Thermophysical, rheological and electrical properties of mono and hybrid TiB 2 / B 4 C nano fl uids based on a propylene glycol : water mixture, Powder Technol. 395 (2022) 391–399, https://doi.org/10.1016/j.powtec.2021.09.074.
[43] M. Ghazvini, M.A. Akhavan-Behabadi, E. Rasouli, M. Raisee, Heat transfer properties of nanodiamond-engine oil nanofluid in laminar flow, Heat Transf. Eng. 33 (6) (2012) 525–532, https://doi.org/10.1080/01457632.2012.624858.
[44] M. Saeedinia, M.A. Akhavan-Behabadi, P. Razi, Thermal and rheological characteristics of CuO-Base oil nanofluid flow inside a circular tube, Int. Commun. Heat Mass Transf. 39 (1) (2012) 152–159, https://doi.org/10.1016/j.icheatmasstransfer.2011.08.001.
[45] M. Fakoor Pakdaman, M.A. Akhavan-Behabadi, P. Razi, An experimental investigation on thermo-physical properties and overall performance of MWCNT/heat transfer oil nanofluid flow inside vertical helically coiled tubes, Exp. Therm. Fluid Sci. 40 (2012) 103–111, https://doi.org/10.1016/j.expthermflusci.2012.02.005.
[46] K. Khanafer, F. Tavakkoli, K. Vafai, A. AlAmiri, A critical investigation of the anomalous behavior of molten salt-based nanofluids, Int. Commun. Heat Mass Transf. 69 (Oct 2015) 51–58, https://doi.org/10.1016/j.icheatmasstransfer.2015.10.002.
[47] M. Chieruzzi, G.F. Cerritelli, A. Miliozzi, J.M. Kenny, Effect of nanoparticles on heat capacity of nanofluids based on molten salts as PCM for thermal energy storage, Nanoscale Res. Lett. 8 (1) (2013) 1–9, https://doi.org/10.1186/1556-276X-8-448.
[48] Q. Xie, Q. Zhu, Y. Li, Thermal Storage Properties of Molten Nitrate Salt-Based Nanofluids with Graphene Nanoplatelets, Nanoscale Res. Lett. 11 (1) (2016) 306, https://doi.org/10.1186/s11671-016-1519-1.
[49] H. Adun, I. Wole-Osho, E.C. Okonkwo, D. Kavaz, M. Dagbasi, A critical review of specific heat capacity of hybrid nanofluids for thermal energy applications, J. Mol. Liq. 340 (2021) 116890, https://doi.org/10.1016/j.molliq.2021.116890.
[50] H. Riazi, S. Mesgari, N.A. Ahmed, R.A. Taylor, The effect of nanoparticle morphology on the specific heat of nanosalts, Int. J. Heat Mass Transf. 94 (2016) 254–261, https://doi.org/10.1016/j.ijheatmasstransfer.2015.11.064.
[51] B. Dudda and D. Shin, "Imece2012-87707 Investigation of Molten Salt Nanomaterial As Thermal Energy Storage in," pp. 1–6, 2012.
[52] Z. Jiang et al., Novel key parameter for eutectic nitrates based nanofluids selection for concentrating solar power (CSP) system, Appl. Energy 235 (July 2019) 529–542, https://doi.org/10.1016/j.apenergy.2018.10.114.
[53] N. Navarrete, L. Hernández, A. Vela, R. Mondragón, Influence of the production method on the thermophysical properties of high temperature molten salt-based nanofluids, J. Mol. Liq. 302 (2020) 112570, https://doi.org/10.1016/j.molliq.2020.112570.
[54] U. Nithiyanantham, L. González-Fernández, Y. Grosu, A. Zaki, J.M. Igartua, A. Faik, Shape effect of Al2O3 nanoparticles on the thermophysical properties and viscosity of molten salt nanofluids for TES application at CSP plants, Appl. Therm. Eng. 169 (2020) 114942, https://doi.org/10.1016/j.applthermaleng.2020.114942.
[55] B. Muñoz-Sánchez, J. Nieto-Maestre, I. Iparraguirre-Torres, J.E. Julià, A. García-Romero, Silica and alumina nano-enhanced molten salts for thermal energy storage: A comparison, AIP Conf. Proc. 1850 (June 2017), https://doi.org/10.1063/1.4984439.
[56] A. Awad, H. Navarro, Y. Ding, D. Wen, Thermal-physical properties of nanoparticle-seeded nitrate molten salts, Renew. Energy 120 (2018) 275–288, https://doi.org/10.1016/j.renene.2017.12.026.
[57] N. Navarrete, R. Mondragón, D. Wen, M.E. Navarro, Y. Ding, J.E. Juliá, Thermal energy storage of molten salt –based nanofluid containing nano-encapsulated metal alloy phase change materials, Energy 167 (2019) 912–920, https://doi.org/10.1016/j.energy.2018.11.037.

[58] Y. Luo, G. Ran, N. Chen, C. Wang, Microstructure and morphology of Mo-based Tm2O3 composites synthesized by ball milling and sintering, Adv. Powder Technol. 28 (2) (2017) 658–664, https://doi.org/10.1016/j.apt.2016.12.003.
[59] N. Navarrete, D. La Zara, A. Goulas, D. Valdesueiro, L. Hernández, J.R. van Ommen, R. Mondragón, Improved thermal energy storage of nanoencapsulated phase change materials by atomic layer deposition, Solar Energy Materials and Solar Cells 206 (2020) 110322, https://doi.org/10.1016/j.solmat.2019.110322.
[60] N.A. Che Sidik, M. Mahmud Jamil, W.M.A. Aziz Japar, I. Muhammad Adamu, A review on preparation methods, stability and applications of hybrid nanofluids, Renew. Sustain. Energy Rev. 80 (May 2017) 1112–1122, https://doi.org/10.1016/j.rser.2017.05.221.
[61] A.H. Pordanjani, S. Aghakhani, M. Afrand, M. Sharifpur, J.P. Meyer, H. Xu, H.M. Ali, N. Karimi, G. Cheraghian, Nanofluids: Physical phenomena, applications in thermal systems and the environment effects- a critical review, J. Clean. Prod. 320 (2021) 128573, https://doi.org/10.1016/j.jclepro.2021.128573.
[62] N. Sezer, M.A. Atieh, M. Koc, A comprehensive review on synthesis, stability, thermophysical properties, and characterization of nanofluids, Powder Technol. 344 (2018) 404–431, https://doi.org/10.1016/j.powtec.2018.12.016.
[63] "Standard Practice for Reducing Samples of Aggregate to Testing Size 1," *Astm C 702 - 9*, vol. 04, no. Reapproved, pp. 700–703, 2003.
[64] D.R. Tobergte, S. Curtis, SODIUM NITRATE FOR HIGH TEMPERATURE LATENT HEAT STORAGE, J. Chem. Inf. Model. 53 (9) (2013) 1689–1699, https://doi.org/10.1017/CBO9781107415324.004.
[65] R. Sabbah, A. Xu-Wu, J.S. Chickos, M.L.P. Leitão, M.V. Roux, L.A. Torres, Reference materials for calorimetry and differential thermal analysis, Thermochim. Acta 331 (2) (1999) 93–204, https://doi.org/10.1016/s0040-6031(99)00009-x.
[66] M. Zappa and M. Schubnell, "Measurement Uncertainty in Thermal Analysis," *METTLER TOLEDO Therm. Anal. Newsl. 3/2020 Meas.*, 2020.
[67] T. Hastie, R. Tibshirani, J. Friedman, The Elements of Statistical Learning, Inference, and Prediction, Second Edi. Springer, Data mining, 2009.
[68] S. Lem, P. Onghena, L. Verschaffel, W. Van Dooren, The heuristic interpretation of box plots, Learn. Instr. 26 (2013) 22–35, https://doi.org/10.1016/j.learninstruc.2013.01.001.
[69] M. Abd-Elghany, T.M. Klapötke, A review on differential scanning calorimetry technique and its importance in the field of energetic materials, Phys. Sci. Rev. 3 (4) (2018) 1–14, https://doi.org/10.1515/psr-2017-0103.
[70] M. Chieruzzi, A. Miliozzi, T. Crescenzi, L. Torre, J.M. Kenny, A New Phase Change Material Based on Potassium Nitrate with Silica and Alumina Nanoparticles for Thermal Energy Storage, Nanoscale Res Lett 10 (1) (2015) 984, https://doi.org/10.1186/s11671-015-0984-2.
[71] Y. Luo, X. Du, A. Awad, D. Wen, Thermal energy storage enhancement of a binary molten salt via in-situ produced nanoparticles, Int. J. Heat Mass Transf. 104 (2017) 658–664, https://doi.org/10.1016/j.ijheatmasstransfer.2016.09.004.
[72] M. Lasfargues, Q. Geng, H. Cao, Y. Ding, Mechanical dispersion of nanoparticles and its effect on the specific heat capacity of impure binary nitrate salt mixtures, Nanomaterials 5 (3) (2015) 1136–1146, https://doi.org/10.3390/nano5031136.
[73] Y. Li, X. Chen, Y. Wu, Y. Lu, R. Zhi, X. Wang, C. Ma, Experimental study on the effect of SiO 2 nanoparticle dispersion on the thermophysical properties of binary nitrate molten salt, Sol. Energy 183 (2019) 776–781, https://doi.org/10.1016/j.solener.2019.03.036.
[74] G. Qiao, M. Lasfargues, A. Alexiadis, Y. Ding, Simulation and experimental study of the specific heat capacity of molten salt based nanofluids, Appl. Therm. Eng. 111 (2017) 1517–1522, https://doi.org/10.1016/j.applthermaleng.2016.07.159.
[75] P.D. Myers, T.E. Alam, R. Kamal, D.Y. Goswami, E. Stefanakos, Nitrate salts doped with CuO nanoparticles for thermal energy storage with improved heat transfer, Appl. Energy 165 (2016) 225–233, https://doi.org/10.1016/j.apenergy.2015.11.045.
[76] T. Bauer, D. Laing, R. Tamme, Characterization of sodium nitrate as phase change material, Int. J. Thermophys. 33 (1) (2012) 91–104, https://doi.org/10.1007/s10765-011-1113-9.
[77] B. Muñoz-Sánchez, J. Nieto-Maestre, G. Imbuluzqueta, I. Marañón, I. Iparraguirre-Torres, A. García-Romero, A precise method to measure the specific heat of solar salt-based nanofluids, J. Therm. Anal. Calorim. 129 (2) (2017) 905–914, https://doi.org/10.1007/s10973-017-6272-x.
[78] I.M. Shahrul, I.M. Mahbubul, S.S. Khaleduzzaman, R. Saidur, M.F.M. Sabri, A comparative review on the specific heat of nanofluids for energy perspective, Renew. Sustain. Energy Rev. 38 (2014) 88–98, https://doi.org/10.1016/j.rser.2014.05.081.
[79] X. Chen, Y.-t. Wu, L.-d. Zhang, X. Wang, C.-f. Ma, Experimental study on thermophysical properties of molten salt nanofluids prepared by high-temperature melting, Sol. Energy Mater. Sol. Cells 191 (2019) 209–217, https://doi.org/10.1016/j.solmat.2018.11.003.
[80] M. Lasfargues, G. Stead, M. Amjad, Y. Ding, D. Wen, In situ production of copper oxide nanoparticles in a binary molten salt for concentrated solar power plant applications, Mat. (Basel) 10 (5) (2017) 1–10, https://doi.org/10.3390/ma10050537.
[81] E. Leonardi, A. Floris, S. Bose, B. D'Aguanno, Unified Description of the Specific Heat of Ionic Bulk Materials Containing Nanoparticles, ACS Nano 15 (1) (2021) 563–574, https://doi.org/10.1021/acsnano.0c0589210.1021/acsnano.0c05892.s001.